

Towards Real-time Text-driven Image Manipulation with Unconditional Diffusion Models

Nikita Starodubtsev*
Yandex

Dmitry Baranchuk
Yandex

Valentin Khruklov
Yandex

Artem Babenko
Yandex

Abstract

Recent advances in diffusion models enable many powerful instruments for image editing. One of these instruments is text-driven image manipulations: editing semantic attributes of an image according to the provided text description. Existing diffusion-based methods already achieve high-quality image manipulations for a broad range of text prompts. However, in practice, these methods require high computation costs even with a high-end GPU. This greatly limits potential real-world applications of diffusion-based image editing, especially when running on user devices.

In this paper, we address efficiency of the recent text-driven editing methods based on unconditional diffusion models and develop a novel algorithm that learns image manipulations 4.5–10× faster and applies them 8× faster. We carefully evaluate the visual quality and expressiveness of our approach on multiple datasets using human annotators. Our experiments demonstrate that our algorithm achieves the quality of much more expensive methods. Finally, we show that our approach can adapt the pretrained model to the user-specified image and text description on the fly just for ~4 seconds. In this setting, we notice that more compact unconditional diffusion models can be considered as a rational alternative to the popular text-conditional counterparts.

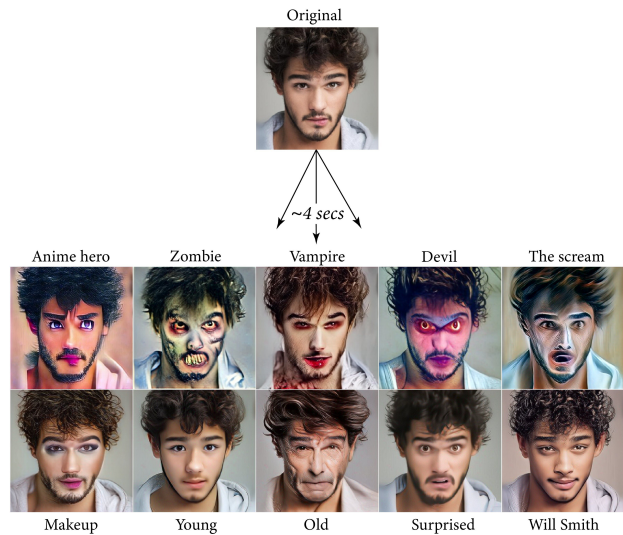


Figure 1: **Few examples of single image editing.** A user provides an image and a text description of the desired transform. Our diffusion-based approach adapts the pretrained model to the given image and text and returns the manipulated image. The entire procedure takes ~4 seconds.

1. Introduction

Diffusion probabilistic models (DPMs) have recently shown remarkable results in image generation, producing both realistic and diverse samples [15, 39]. After their initial success, diffusion models have seen use in many related applications, including object detection [7], semantic segmentation [5], image processing [37, 26] and many others.

One popular application of diffusion models is text-guided image manipulation, where DPM is used to edit an existing image, changing its attributes to match a user-specified

text description. This application has become a hot topic after the appearance of high-quality text-conditional DPMs like Imagen [36], DALL-E 2 [33], Stable Diffusion [34].

Text-conditional DPMs are trained on large and diverse datasets with rich text information, such as MS-COCO [24] or LAION5B [38], and applicable to a wide range of domains at a time. However, some practical applications focus solely on some simple and narrow domain, e.g., human faces, and often have strict computational budgets. In these cases, unconditional diffusion models might be a reasonable alternative since they already provide strong generative performance on such domains being more efficient than large and diverse text-conditional models. Moreover, unconditional models avoid tedious text annotation process that increases the costs and can raise additional legal and ethical concerns.

Several recent works have learned text-driven image

*Correspondence to nstarodubtcev@itmo.ru

manipulations using only unconditional generative models. Some methods use unconditional GANs [19, 18], showing strong results for text-driven domain adaptation [12, 3, 2] and single image editing [31]. Other works [20, 23] exploit unconditional diffusion models, significantly outperforming GANs in terms of both image fidelity and editing quality.

However, compared to GANs, diffusion-based image manipulations require expensive sequential inversion and generation, limiting their applicability in resource-limited environments. Moreover, some applications, e.g., single image editing, also require highly performant online adaptation where current diffusion-based methods are still not efficient enough in terms of both adaptation time and memory usage.

In this work, we analyze the performance bottlenecks of the existing text-guided image manipulation methods based on unconditional diffusion models and propose a workaround to circumvent them. As a result, we present a fast and memory-efficient diffusion-based approach that preserves the visual and editing quality of the prior image manipulation methods.

To sum up, the contributions of the paper are as follows:

- We develop a practical algorithm for text-driven image manipulation based on fast approximate sampling procedures. Our algorithm learns image manipulations 4.5–10× faster and applies them 8× faster than previous methods based on unconditional diffusion models. The source code of our algorithm is available online¹.
- We conduct a thorough human evaluation on multiple standard image datasets to compare the produced image manipulations in terms of visual quality and their correspondence to the text attribute. Our algorithm achieves similar editing quality as significantly more expensive counterparts.
- We observe an emergent property of our training procedure. When the model is trained using our protocol, it also learns to improve the perceptual quality of approximate image estimates without being explicitly enforced to do so. We reveal that it is an implicit side-effect of the directional CLIP loss [12]. From a practical standpoint, this phenomenon helps us to accelerate model inference without perceptible loss in image fidelity.
- We demonstrate that unconditional diffusion models can learn text-guided image manipulations from a single image. This allows users to create their own image transformations on the fly, using the same image they intend to manipulate. For this application, our approach can edit images with significantly better quality than existing GAN-based alternatives. Notably, on narrow domains like human faces, the proposed method can provide reasonable

quality-efficiency trade-off compared to the state-of-the-art text-driven editing methods based on Stable Diffusion.

2. Background

This section provides an overview of diffusion models, briefly discusses previous text-driven image manipulation methods and describes the core aspects of the Diffusion-CLIP [20] approach that is mostly leveraged in our work.

2.1. Diffusion probabilistic models

Diffusion models [15] are latent variable generative models trained to approximate the data distribution $x_0 \sim q(x_0)$ by using *forward* and *reverse* diffusion processes.

The forward diffusion process $q(x_{1:T}|x_0)$ gradually applies Gaussian noise with some predefined variance schedule β to a real image x_0 until it converges to isotropic Gaussian distribution $x_T \sim N(0, I)$. A latent variable x_t can be sampled directly from x_0 in the closed form:

$$q(x_t|x_0) = \mathcal{N}(x_t; \sqrt{\bar{\alpha}_t}x_0, 1 - \bar{\alpha}_tI), \quad (1)$$

where $\alpha_t := 1 - \beta_t$, $\bar{\alpha}_t := \prod_{s=1}^t \alpha_s$.

The reverse process allows generating new samples from $q(x_0)$ by gradually transforming $x_T \sim N(0, I)$ to x_0 , which requires T neural network forward passes. Often, $T=1000$ and hence the generation takes much more time compared with feed-forward generative models, e.g., GANs [13, 19].

Many recent works have addressed this problem [10, 17, 39, 40, 44, 25] and demonstrated convincing results within a few dozens of inference steps. DDIM [39] is one of the most prevalent samplers that generates plausible samples for $\tau_{dec} \approx 50-100$ steps without re-training the initial model.

In more detail, DDIM obtains a sample x_{t-1} from x_t in the following way:

$$x_0(t; \theta) = \frac{x_t - \sqrt{1 - \alpha_t} \epsilon_\theta(x_t)}{\sqrt{\alpha_t}} \quad (2)$$

$$x_{t-1} = \sqrt{\alpha_{t-1}} \cdot x_0(t; \theta) + \sqrt{1 - \alpha_{t-1}} \epsilon_\theta(x_t) \quad (3)$$

where $x_0(t; \theta)$ is a x_0 estimate at a time step t and $\epsilon_\theta(x_t)$ is a prediction of the noise component using a pretrained diffusion model with parameters θ .

In addition, DDIM is deterministic and serves as a de-facto standard inversion method for diffusion models with low reconstruction errors. Opposed to (1), DDIM has to sequentially apply the pretrained model to map a real image $x_0 \sim q(x_0)$ into the latent variable x_t :

$$x_{t+1} = \sqrt{\alpha_{t+1}} \cdot x_0(t; \theta) + \sqrt{1 - \alpha_{t+1}} \epsilon_\theta(x_t) \quad (4)$$

Thus, the image “inversion” for diffusion models is much more expensive compared with VAEs [21] or GANs [41, 1].

¹<https://github.com/quickjkee/eff-diff-edit>

2.2. Text-guided image manipulation

One of the leading directions for semantic image manipulation with generative models is to use natural language prompts to guide the image generation toward the desired transformation.

The first popular group of methods considers pretrained text-conditional diffusion models [34, 33, 36, 30]. Some of them leverage the internal knowledge of the existing models by manipulating text embeddings [11, 35] or cross attention weights [14, 28]. Other works propose to finetune the model parameters on a single image [46, 42] and perform expressive text-driven manipulations upon it. The recent work [6] finetunes Stable Diffusion on the large set of GPT-3 powered paired examples. This allows them to achieve both efficient and high-quality image transforms.

Another research direction is to exploit pretrained unconditional models along with an external model for text guidance, typically CLIP [32]. In general, the methods encode real images into the model latent space and then either modify the latent representations [23, 31] or the model parameters directly [20, 12] to minimize the CLIP loss.

Although GAN-based methods [31, 12, 3, 2] can provide efficient adaptation and inference, they still suffer from imperfect image inversion and provide less expressive and natural image transformations compared with the diffusion models. On the other hand, DDPM-based methods [20, 23] have to perform costly sequential forward and reverse processes to edit a single image.

There is also a line of work that suggests training an image generator from scratch on a single image [22, 4, 43] and then applying the CLIP model for the text-driven editing. The main limitations of such methods are a time consuming adaptation and a scarce set of available transformations, e.g., style transfer and image harmonization.

2.3. DiffusionCLIP

DiffusionCLIP [20] is a recent approach for text-driven image manipulation using unconditional diffusion models. This method adapts ϵ_θ to a new diffusion model $\epsilon_{\hat{\theta}}$ such that the transformation of a source image x_0 into $x_0(\hat{\theta})$ is associated with the text description y_{tar} , e.g., “Makeup face”.

In more detail, it encodes the image x_0 into the latent variable x_{t_0} using DDIM in forward direction (4) with the original diffusion model ϵ_θ . In practice, the DDIM encoding is applied for some predefined steps $\tau_{enc} \leq t_0$ to obtain x_{t_0} . The typical values of t_0 are within [300, 600]. Lower t_0 is useful for “shallow” image manipulations, e.g., adding makeup. Higher t_0 is required for strong transformations that significantly affect the structure of semantic attributes, e.g., “Person” to “Zombie”.

Then, at each training iteration, DiffusionCLIP transforms x_{t_0} to $x_0(\theta)$ using the DDIM generation (3) for τ_{dec}

steps and backpropagates through the entire decoding process to minimize the following objective:

$$\mathcal{L}(\theta) = \mathcal{L}_{dir}(x_0(\theta), y_{tar}; x_0, y_{ref}) + \lambda \cdot \mathcal{L}_{id}(x_0(\theta); x_0) \quad (5)$$

where \mathcal{L}_{dir} essentially enforces semantic transfer from y_{ref} to y_{tar} and \mathcal{L}_{id} serves to preserve the attributes of the original image x_0 . λ is a hyperparameter that controls the regularization strength. Note that τ_{enc} and τ_{dec} are hyperparameters of the method allowing us to trade reconstruction quality for processing speed; in practice, typical values are $\tau_{enc} \in [40, 200]$ and $\tau_{dec} \in [6, 40]$ [20].

\mathcal{L}_{dir} is a directional CLIP loss [12] which minimizes the cosine distance between cross-domain directions in the CLIP space. Specifically, given the CLIP text encoder E_T , the text direction is defined as $\Delta T = E_T(y_{tar}) - E_T(y_{ref})$, where y_{ref} is a text prompt that represents the source domain in general, e.g., “Person”. The direction between the source x_0 and transformed $x_0(\theta)$ images is defined similarly using the CLIP image encoder E_I : $\Delta I = E_I(x_0(\theta)) - E_I(x_0)$. The overall \mathcal{L}_{dir} objective is calculated as follows:

$$\mathcal{L}_{dir} = 1 - \frac{\langle \Delta T, \Delta I \rangle}{\|\Delta T\|_2 \|\Delta I\|_2} \quad (6)$$

\mathcal{L}_{id} is typically a reconstruction loss in the pixel space: $L_1 = \|x_0(\theta) - x_0\|_1$. Optionally, it may include additional domain specific losses, e.g., $\mathcal{L}_{face}(x_0(\theta), x_0)$ that attempts to preserve the face identity in the image x_0 for the source domain “Person” via a pretrained face recognition network.

Efficiency. The resulting algorithm performs image manipulations with state-of-the-art quality but requires significantly more compute and memory than the GAN-based counterparts. When dealing with 256×256 images, DiffusionCLIP takes minutes to adapt the model to the target transform and a few seconds to apply it to a single image.

During training, DiffusionCLIP unrolls several diffusion steps and backpropagates through the decoding process at each model update step. To allow this backpropagation, it needs to store intermediate model activations from every step, taking up extra GPU memory. Thus, even with a batch size 1, it consumes ~ 21 GiB GPU VRAM and hence cannot fit most end-user GPUs. In contrast, the GAN-based competitor [12] consumes only ~ 3 GiB.

The authors of DiffusionCLIP suggest a possible way to reduce memory consumption by independently updating the model parameters at each decoding step. This strategy halves the overall GPU usage but doubles the training time due to the sequential model update steps.

During inference, the main performance bottleneck is the DDIM encoding that requires running a forward pass of the diffusion model at each step to apply noise to the original image. As a result, the algorithm spends more than half of the total inference time *applying* noise to the image.

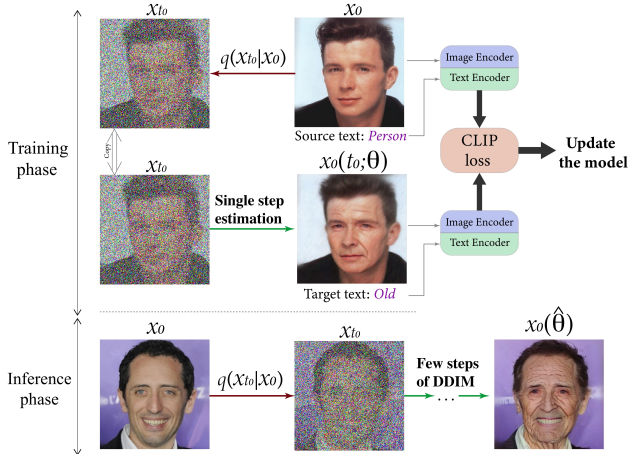


Figure 2: Overview of the proposed approach. **Training phase.** Diffusion model parameters θ are updated to minimize the directional CLIP loss (6) for a single-step x_0 estimate that lack high-frequency perceptual details. **Inference phase.** A real image x_0 is mapped to the latent variable x_{t_0} using the forward diffusion process in the closed-form (1). The edited image is generated for a few steps of the DDIM decoding that sequentially applies the learned transform and recovers the fine-grained details.

3. Method

In this section, we design a more efficient image manipulation algorithm that circumvents the expensive multi-step processing in the DiffusionCLIP training and inference stages. We conjecture that the objective (5) does not need precise image reconstruction $x_0(\theta)$ to successfully learn the text-driven image transformation. We apply this intuition to speed up training and inference in Sections 3.1 and 3.2, respectively. Figure 2 summarizes our approach.

3.1. Single step training

As we describe in Section 2.3, each DiffusionCLIP training step starts with x_{t_0} , applies the DDIM generating process for τ_{dec} steps to obtain $x_0(\theta)$, then uses it to estimate $\mathcal{L}(\theta)$ and backpropagate through the entire computational graph to update parameters θ .

To avoid the costly multi-step procedure, instead of generating an edited image $x_0(\theta)$ for τ_{dec} steps, we estimate the expected x_0 using eq. (2) and denote it as $x_0(t_0; \theta)$. The $x_0(t_0; \theta)$ estimate lacks some fine-grained details. This is illustrated in Figure 3 that presents $x(t_0; \theta)$ predictions for different t_0 steps². However, we hypothesize that our training procedure only needs $x_0(t_0; \theta)$ to preserve the semantic

²The predictions are obtained with a diffusion model pretrained on the CelebA-HQ dataset from <https://github.com/ermongroup/SDEdit>.

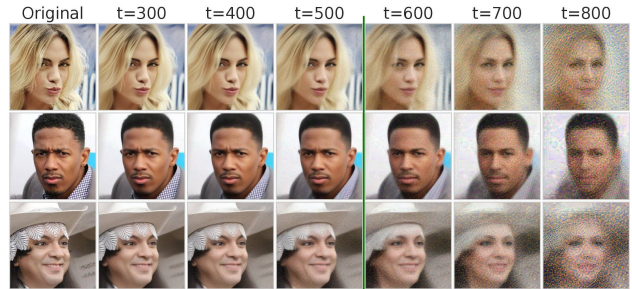


Figure 3: Visualisation of $x_0(t_0; \theta)$ predictions for different t_0 . The estimates for $t_0 \leq 500$ preserve main semantic attributes of the original images.

attributes that are not supposed to be altered during the particular image manipulation.

Since $x_0(t_0; \theta)$ is a *single-step* estimate, the method performs only a single forward and backward pass of the diffusion model per training iteration. This results in both faster training and significantly less memory usage since there is no need to store multi-step activations in GPU memory. We report the exact runtimes and memory usage in Section 4.2.

Emergent effect of the training procedure. Interestingly, aside from the intended purpose of faster training, the proposed algorithm improves the visual quality of the resulting $x_0(t_0; \theta)$ predictions. This effect is not obvious since the objective \mathcal{L} does not have any terms that explicitly optimize the image quality. This phenomenon allows us to reduce the number of DDIM decoding steps τ_{dec} and further speed up the inference. In Section 4.1, we explore this emergent property in more detail.

3.2. Efficient forward processing

In addition, DiffusionCLIP needs the costly DDIM encoding process to precisely invert the sampling procedure up to fine-grained details. We argue that this exact inversion is unnecessary because semantic image manipulations are performed at the middle steps of the diffusion process where most semantic attributes have already been formed. Also, the edit typically requires noticeable image manipulations that override the details generated during the final steps.

Therefore, we suggest replacing the DDIM encoding (3) with the DDPM forward process and sample $x_{t_0} \sim q(x_{t_0} | x_0)$ in the closed-form using eq. (1). Notably, we use the DDPM forward process only for encoding, retaining DDIM for the decoding phase.

In Figure 4, we visualize the image reconstructions $x_0(\theta)$ obtained with DDIM and DDPM encoding methods for different $t_0 \in [300, 600]$ values. We observe that $x_0(\theta)$ reconstructed from $x_{t_0} \sim q(x_{t_0} | x_0)$ are still consistent with x_0 for $t_0 \leq 450$. In Appendix C, we provide the mean opinion score that quantitatively supports this observation.

To sum up, we combine the two modifications above and

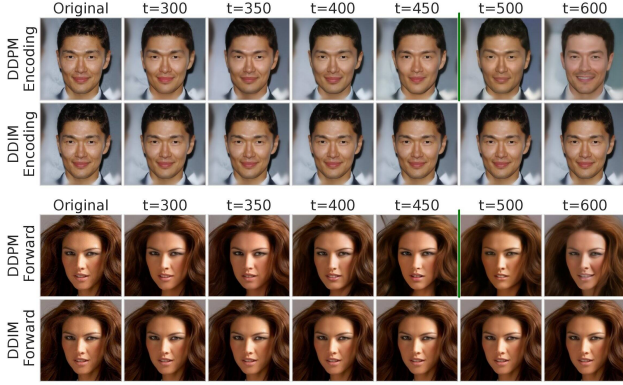


Figure 4: Image reconstruction with stochastic (DDPM) and deterministic (DDIM) encoding methods for different diffusion steps t_0 . The reconstructions obtained from DDPM encodings for $t_0 \leq 450$ are still consistent with the original images and suit well for most image manipulations.

present the overall training algorithm in Appendix A.

During the inference, the proposed method encodes an image x_0 into the latent variable $x_{t_0} \sim q(x_{t_0}|x_0)$ and uses the DDIM decoding for τ_{dec} steps to gradually apply the learned manipulation and recover high-frequency details.

4. Experiments

In this section, we first investigate the emergent effect caused by our training procedure. Then, we evaluate the efficiency of our approach in comparison with DiffusionCLIP and GAN-based alternatives. Finally, we demonstrate the qualitative and quantitative results of our approach for the following settings:

- **Prelearned image manipulations** — the model is first adapted to the text description on 50 images. Then, the learned transform is applied to the hold-out images.
- **Single-image editing** — the model is adapted to the user-specified text description and image on the fly.

4.1. Analysis

Quality improvement effect. As we discuss in Section 3.1, the proposed training procedure demonstrates an interesting phenomenon: optimizing \mathcal{L}_{dir} improves the perceptual quality of the $x_0(t_0; \hat{\theta})$ estimate after the model adaptation. Thanks to this effect, our method can produce samples of the same visual quality for $\tau_{dec}=6$ steps instead of 40 considered in the best DiffusionCLIP configuration.

In Figure 5, we measure the dynamics of $x_0(t_0, \hat{\theta})$ quality w.r.t. different fine-tune iterations using NIQE [27] — the established metric for the no-reference image quality assessment. Opposed to DiffusionCLIP, we observe that the quality of the x_0 estimates indeed significantly increases over training for our method.

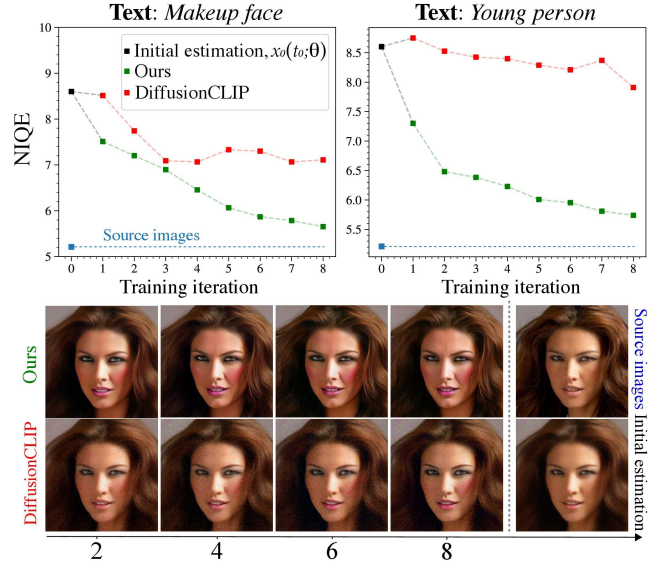


Figure 5: Image quality (NIQE) of $x_0(t_0; \hat{\theta})$ estimate w.r.t. training iterations. For both methods, the estimates get better but improvements are way more pronounced for the proposed method.

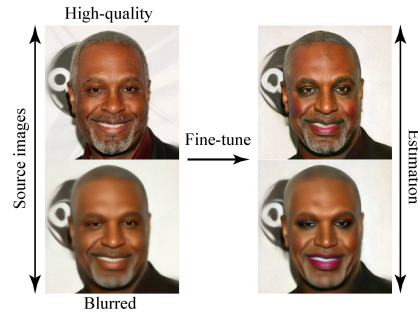


Figure 6: Visualization of $x_0(t_0; \hat{\theta})$ estimates after fine-tuning for x_0 of different perceptual quality. The estimates tend to inherit the perceptual details of the source images.

What causes improvement of $x_0(t_0; \hat{\theta})$? The directional CLIP loss (6) aims to move the image embedding of the $x_0(t_0; \hat{\theta})$ estimate to make a vector $E_I(x_0(t_0; \hat{\theta})) - E_I(x_0)$ co-directional to the text direction $E_T(y_{ref}) - E_T(y_{tar})$ in the CLIP embedding space.

We hypothesize that the x_0 transformations along the text direction weakly correlate to the perceptual quality unless it is assumed by the manipulation. If so, the quality of the $x_0(t_0; \hat{\theta})$ is essentially determined by the source image x_0 .

To confirm our assumption, we first consider some text direction, e.g., “Face” to “Makeup Face” and optimize \mathcal{L}_{dir} for x_0 and its manually blurred version x_0^{blur} , independently. In Figure 6, we visualize $x_0(t_0; \hat{\theta})$ estimates after the model adaptation. We observe that the estimates tend to preserve the sharpness of the source images.

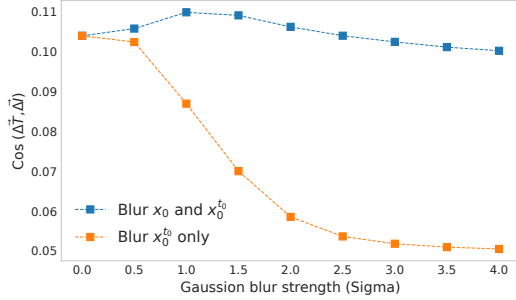


Figure 7: Cosine between ΔT and ΔI directions in the CLIP space w.r.t. Gaussian blur strength applied to the image x_0 and its manipulated estimate $x_0(t_0; \hat{\theta})$. The angle is not affected much if both x_0 and $x_0(t_0; \hat{\theta})$ are corrupted equally. This indicates that the semantic direction induced by ΔT has weak correlation with the image quality direction.

Method	Encoding, sec	Decoding, sec
StyleGAN-NADA	0.29	0.07
DiffusionCLIP	1.53	0.22
Ours	0.00	0.22

Table 1: The time spent to encode and decode a single image of 256×256 resolution at the inference stage.

Secondly, we explore the behavior of the semantic direction when the perceptual quality of the target and source images changes. In more detail, we consider source images x_0 and their $x_0(t_0; \hat{\theta})$ estimates after the model adaptation. In the first setting, we fix x_0 and apply Gaussian blur of different degree only to $x_0(t_0; \hat{\theta})$: $\Delta I(x_0, x_0^{blur}(t_0; \hat{\theta}))$. In the second setting, we apply Gaussian blur to both x_0 and $x_0(t_0; \hat{\theta})$: $\Delta I(x_0^{blur}, x_0^{blur}(t_0; \hat{\theta}))$. We consider Gaussian blur with kernel size 7 and vary sigma from 0 to 4. Then, we measure cosine between the image direction ΔI and the text direction ΔT for various y_{tar} . The results are averaged over 6 transforms and presented in Figure 7. We observe that the image direction ΔI does not noticeably change if both images are equally corrupted.

4.2. Training and inference efficiency

Setting. The proposed method and DiffusionCLIP exploit the same pretrained models. As a GAN-based baseline, we consider StyleGAN-NADA [12] that is built upon the StyleGAN2 [19] generator. In this evaluation, all models are pretrained on CelebA-HQ and operate on 256×256 images.

All measurements are performed in an isolated environment on a single NVIDIA A100 GPU and averaged over 10 independent runs. For both baselines, we consider the official implementations and the best settings described in the corresponding papers. We provide the exact hardware and software configuration in Appendix B.

Training efficiency. We start with the evaluation of the training performance of each method. The training set con-

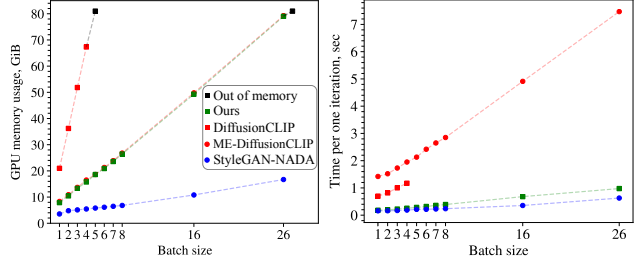


Figure 8: Comparison of our approach, DiffusionCLIP and StyleGAN-NADA in terms GPU memory usage (GiB) (Left) and run-times (sec) (Right) for a single training iteration.

tains 50 images.

The first phase is to precompute the latent variables x_{t_0} for all training images x_0 . DiffusionCLIP exploits the DDIM encoding for $\tau_{enc}=40$ steps and spends ~ 67 seconds to encode 50 images. On the other hand, our method gets x_{t_0} in the closed form. StyleGAN-NADA is trained on self-generated samples and hence skips this phase.

Then, in Figure 8, we compare the GPU memory consumption (Left) and runtime (Right) of a single training iteration w.r.t. different batch sizes. As an additional baseline, we consider the memory efficient (ME) DiffusionCLIP procedure described in Section 2.3. During the training, DiffusionCLIP performs $\tau_{gen}=6$ decoding steps.

We observe that our approach is significantly faster than both DiffusionCLIP versions. For example, our method demonstrates 0.18s against 0.70s and 1.42s for DiffusionCLIP and ME-DiffusionCLIP, respectively. Notice that the gap increases with a batch size.

In terms of GPU memory usage, our procedure consumes 7GiB for a batch size 1 that is 14GiB less compared with the original DiffusionCLIP method. Moreover, DiffusionCLIP exceeds the GPU memory limit (> 80 GiB) for a batch size 5 while our method consumes only ~ 18 GiB and meets OOM only for a batch size 27. ME-DiffusionCLIP consumes similar GPU memory to our method because both perform a model update only for a single diffusion step at a time. On the contrary, StyleGAN-NADA is still noticeably more memory efficient than diffusion-based alternatives, especially for large batch sizes.

Finally, we measure the overall training performance. DiffusionCLIP and our method perform 1–10 training epochs depending on the target transform. Thus, for a batch size 1, our procedure spends from 10.7 seconds to 1.58 minutes, while the fastest DiffusionCLIP procedure spends from 101 seconds to 7.2 minutes. Note that the efficiency gains increase for larger batch sizes.

StyleGAN-NADA requires 50–300 training iterations and operates on a batch size 2. In this case, the overall training takes from 8.1 seconds to 58.5 seconds.

In the result, our training procedure is $4.5\text{--}10\times$ faster and consumes 14GiB less GPU memory than original DiffusionCLIP and $8\text{--}18\times$ faster than its memory efficient alternative. In comparison with StyleGAN-NADA, our adaptation still consumes extra 4 GiB memory but, notably, is comparable in terms of the training time.

Inference time. Then, we compare the method performance at the inference stage. The fastest DiffusionCLIP configuration considers $\tau_{enc}=40$ encoding steps and the $\tau_{dec}=6$ for decoding. Our approach encodes an image for free and performs $\tau_{dec}=6$ decoding steps. StyleGAN-NADA utilizes Restyle [1] + e4e [41] as an encoding method.

The results are presented in Table 1. As one can see, our approach with efficient approximate encoding results in $8\times$ faster inference than DiffusionCLIP. Moreover, it also demonstrates $\sim 50\%$ speedup compared to StyleGAN-NADA due to the costly image encoder.

4.3. Prelearned image manipulations

For this setting, we evaluate the quality of the image manipulations on the Celeba-HQ-256 [16], AFHQ-dog-256 [8], LSUN-Church-256 [45] and ImageNet-512 [9] datasets. As baseline methods, we consider DiffusionCLIP, StyleGAN-NADA, Asyrp [23] and HyperDomainNet [3]. For each method, we consider the hyperparameter values from the corresponding official implementations and papers. If some hyperparameters are missing, we carefully tune them by ourselves. For DiffusionCLIP, opposed to the fastest setting with $\tau_{dec}=6$ in Section 4.2, in this experiment, we set $\tau_{dec}=40$ during the inference to derive the best editing results. Note that our approach still performs $\tau_{dec}=6$ decoding steps. For comparison, we use 35 images from the test sets. 16 text descriptions are taken for Celeba-HQ-256 and 6 for other datasets. The list of textual transforms is in Appendix D.1.

As a primary quality measure, we consider a side-by-side human evaluation. Specifically, we provide a source image, text description and images edited with two different methods and then ask people to answer two questions: 1) *Which of the edited images corresponds better to the text description?* and 2) *Which of the edited images has more artifacts and changes that are not related to the text?*. In total, we collect 9500 votes. The voting results are presented in Table 2. Figure 9 provides the visualizations for various transformations. More visual examples are in Figures 16, 17, 18, 19, 20, 21. The qualitative comparison with HyperDomainNet [3] is presented in Figure 22.

Compared with DiffusionCLIP, our approach corresponds better to the text attributes on Celeba-HQ and LSUN-Church. On other datasets, the votes are distributed equally. In terms of artifacts, we observe parity between both methods. This means that our method still produces high-fidelity images and provides as expressive image transforms as DiffusionCLIP. Moreover, despite using stochastic encoding, our al-

Dataset	Ours, %	Both, %	DiffusionCLIP, %
<i>Q1. Which one corresponds better to the text?</i>			
Celeba-HQ	54.21 \pm 1.82	5.96 \pm 1.23	39.82 \pm 2.68
AFHQ-Dog	44.11 \pm 3.25	16.74 \pm 4.65	38.85 \pm 2.12
ImageNet	35.42 \pm 4.11	31.23 \pm 1.96	33.23 \pm 3.37
LSUN-Church	40.67 \pm 3.85	18.95 \pm 1.39	40.38 \pm 3.22
<i>Q2. Which one has more text-irrelevant changes?</i>			
Celeba-HQ	40.53 \pm 1.89	20.60 \pm 2.05	38.85 \pm 1.95
AFHQ-Dog	40.28 \pm 3.53	21.43 \pm 4.52	37.70 \pm 3.07
ImageNet	39.90 \pm 4.19	21.90 \pm 4.71	38.19 \pm 4.62
LSUN-Church	35.23 \pm 1.78	28.28 \pm 1.98	36.47 \pm 1.98

Dataset	Ours, %	Both, %	StyleGAN-NADA, %
<i>Q1. Which one corresponds better to the text?</i>			
Celeba-HQ	57.26 \pm 1.65	6.65 \pm 0.20	35.95 \pm 1.61
LSUN-Church	69.04 \pm 3.75	9.05 \pm 1.85	21.23 \pm 2.67
<i>Q2. Which one has more text-irrelevant changes?</i>			
Celeba-HQ	29.06 \pm 2.06	21.79 \pm 2.17	48.89 \pm 0.72
LSUN-Church	18.76 \pm 3.28	19.23 \pm 1.82	62.01 \pm 3.71

Dataset	Ours, %	Both, %	Asyrp, %
<i>Q1. Which one corresponds better to the text?</i>			
Celeba-HQ	81.50 \pm 6.6	5.53 \pm 1.92	13.05 \pm 5.83
<i>Q2. Which one has more text-irrelevant changes?</i>			
Celeba-HQ	21.50 \pm 5.36	22.06 \pm 6.00	57.01 \pm 8.77

Dataset	Ours, %	Both, %	HyperDomainNet, %
<i>Q1. Which one corresponds better to the text?</i>			
Celeba-HQ	56.72 \pm 3.13	2.53 \pm 2.02	40.83 \pm 1.34
<i>Q2. Which one has more text-irrelevant changes?</i>			
Celeba-HQ	36.75 \pm 1.56	22.50 \pm 4.33	40.81 \pm 2.24

Table 2: Side-by-side human evaluation of various image manipulations learned with the proposed, DiffusionCLIP, Asyrp and StyleGAN-NADA approaches. Our method preserves quality of DiffusionCLIP and significantly outperforms other methods according to both criteria.

gorithm does not induce noticeable artifacts in semantic attributes: even for the shallow transformations, e.g., “Makeup face”, images still preserve important source details.

Against StyleGAN-NADA, Asyrp and HyperDomainNet, the proposed method significantly outperforms all of them according to both criteria.

4.4. Single-image editing

In this experiment, we make use of a significantly more efficient training procedure and consider our approach for text-driven single-image editing.

In this setting, we consider Celeba-HQ-256 and compare our method with DiffusionCLIP, StyleGAN-NADA and StyleCLIP [31] — GAN-based approach that allows fast single-image editing.

In addition, popular text-conditional models also offer the tools to edit a single image for the user-specified text description. Therefore, we compare our method with recent

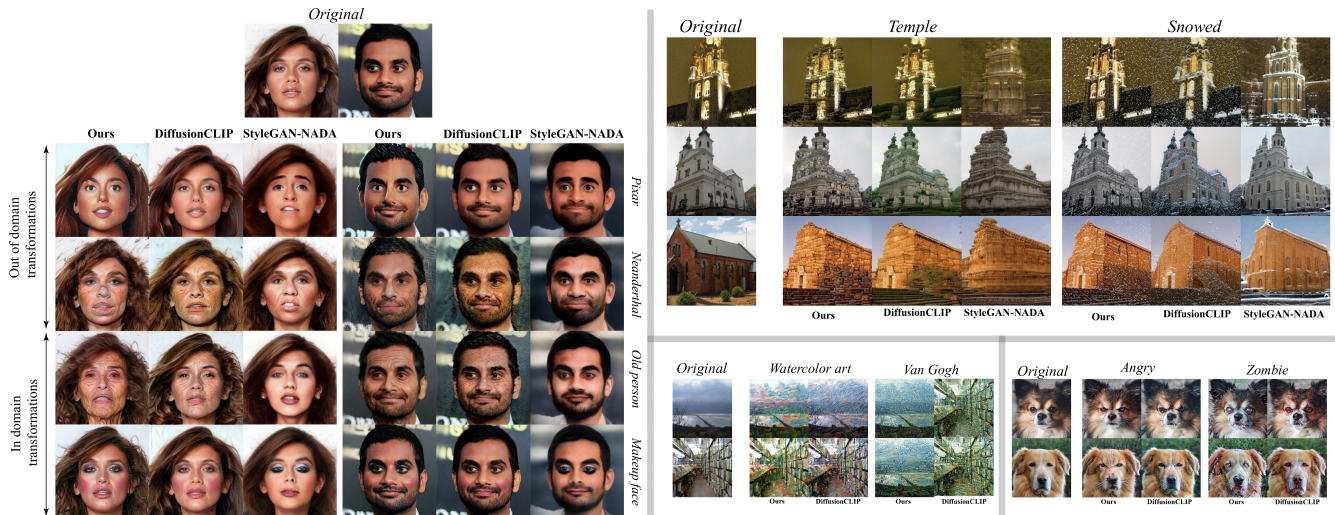


Figure 9: Visual examples of the image manipulations learned with the DiffusionCLIP, StyleGAN-NADA and our approaches for the Celeba-HQ-256, LSUN-church-256, AFHQ-dog-256 and ImageNet-512 datasets.

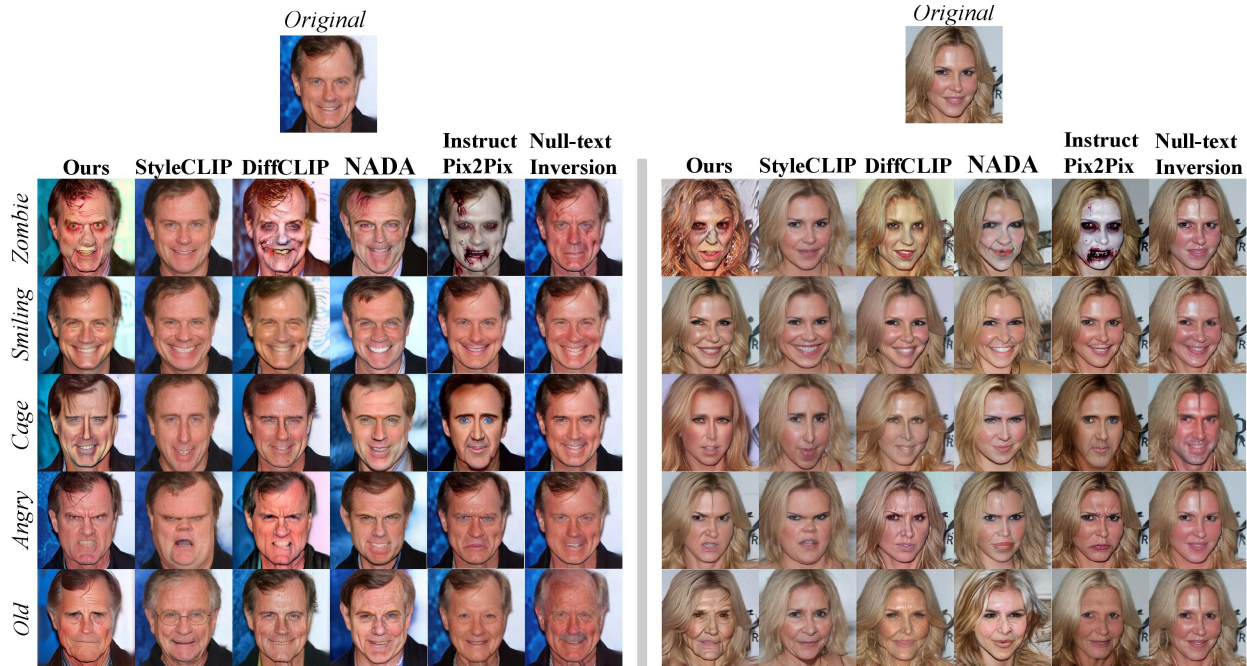


Figure 10: Visual examples produced with different single-image editing approaches. Our method, DiffusionCLIP, StyleCLIP and StyleGAN-NADA represent the methods using unconditional generative models. InstructPix2Pix and Null-text Inversion methods are based on Stable Diffusion.

editing methods [28, 6] based on Stable Diffusion [34].

First, we measure the overall time to apply the transform to a source image. DiffusionCLIP and our approach require ~ 20 training iterations for high quality adaptation. StyleGAN-NADA starts producing reasonable image transforms for 150 training iterations. Overall, our method, DiffusionCLIP, StyleGAN-NADA and StyleCLIP demonstrate 3.8, 14.9, 35.8 and 1.1 seconds per image, respectively. Null-

text inversion [28] requires 40–120 seconds to edit a single image. On the other hand, InstructPix2Pix [6] performs text-guided editing for a single forward pass of Stable Diffusion which takes ~ 9 seconds.

Then, we evaluate the visual quality of the manipulated images. We consider 6 images and 8 in-domain and 8 out-of-domain textual transforms. The full list of textual transforms is in Appendix D.2. The results for some of them are pre-

	Ours, %	Both, %	DiffusionCLIP, %
Text correspondence	60.20 \pm 3.80	5.05 \pm 2.30	34.74 \pm 5.81
More irrelevant changes	36.56 \pm 4.06	26.46 \pm 4.39	36.76 \pm 5.73
	Ours, %	Both, %	StyleCLIP, %
Text correspondence	53.33 \pm 6.40	10.41 \pm 3.49	36.25 \pm 8.89
More irrelevant changes	27.50 \pm 4.25	23.33 \pm 6.89	49.17 \pm 3.86
	Ours, %	Both, %	StyleGAN-NADA, %
Text correspondence	71.57 \pm 5.22	7.84 \pm 2.70	20.58 \pm 3.82
More irrelevant changes	35.68 \pm 3.59	19.21 \pm 3.73	45.09 \pm 2.40
	Ours, %	Both, %	Null-text Inversion, %
Text correspondence	68.32 \pm 6.85	5.81 \pm 2.00	25.81 \pm 3.82
More irrelevant changes	42.31 \pm 6.71	16.84 \pm 8.73	40.82 \pm 8.62
	Ours, %	Both, %	InstructPix2Pix, %
Text correspondence	36.88 \pm 4.50	6.25 \pm 2.38	56.88 \pm 4.30
More irrelevant changes	52.63 \pm 4.47	16.32 \pm 1.97	31.05 \pm 2.86

Table 3: Side-by-side human evaluation for single-image editing on CelebA-HQ-256. Our method outperforms DiffusionCLIP and Null-text Inversion according to text correspondence and GAN-based methods according to both criteria. InstructPix2Pix provides better editing results for most transforms.

sented in Figure 10. More examples for various textual transforms are in Figures 23, 24.

Also, we run the side-by-side comparison collecting 1860 votes for all evaluations and present the results in Table 3. Note that StyleCLIP is not designed to handle out-of-domain manipulations, e.g., “Person” to “Zombie”. Therefore, for a fair evaluation, we compare our method to StyleCLIP only on the in-domain transformations.

We observe that our training procedure demonstrates higher text correspondence compared to DiffusionCLIP under the same level of artifacts and significantly outperforms all GAN-based methods according to both criteria.

For Null-text Inversion, we also select 6 out of 16 transforms for which it is able to produce reasonable manipulation results. For these transforms, our method still provides more expressive results under the same level of text-irrelevant changes.

Our strongest competitor, InstructPix2Pix demonstrates impressive results for most transforms in our evaluation. However, we notice that there are some transforms where InstructPix2Pix produces either too weak or too unrealistic results, e.g., “Smiling person”, “Surprised person” or “Makeup face”.³ Therefore, if one wants to add new manipulations, one needs to reproduce the entire pipeline of InstructPix2Pix training that includes incredibly expensive data collection and adaptation procedures. In contrast, our method uses the pretrained diffusion model out-of-the-box and needs only a single image to learn the desired transform. Notably, our approach provides reasonable image manipula-

³We followed the tips provided by the authors but still could not get plausible results.

tions for all considered transforms. More visual examples in comparison with InstructPix2Pix are in Figure 24.

5. Conclusion

This work addresses the inefficiency of existing image manipulation approaches built upon unconditional diffusion models. We observe that image manipulations can be efficiently learned on inaccurate source image predictions without noticeable loss in perceptual and editing quality. In the result, we obtain a highly performant and memory-efficient procedure that can be further considered for real-world applications looking for expressive and efficient image manipulation methods.

References

- [1] Yuval Alaluf, Or Patashnik, and Daniel Cohen-Or. Restyle: A residual-based stylegan encoder via iterative refinement. In *Proceedings of the IEEE/CVF International Conference on Computer Vision (ICCV)*, October 2021. 2, 7
- [2] Yuval Alaluf, Or Patashnik, Zongze Wu, Asif Zamir, Eli Shechtman, Dani Lischinski, and Daniel Cohen-Or. Third time’s the charm? image and video editing with stylegan3, 2022. 2, 3
- [3] Aibek Alanov, Vadim Titov, and Dmitry P. Vetrov. Hyperdomainnet: Universal domain adaptation for generative adversarial networks. In Alice H. Oh, Alekh Agarwal, Danielle Belgrave, and Kyunghyun Cho, editors, *Advances in Neural Information Processing Systems*, 2022. 2, 3, 7
- [4] Omer Bar-Tal, Dolev Ofri-Amar, Rafail Fridman, Yoni Kasten, and Tali Dekel. Text2live: Text-driven layered image and video editing. In *European Conference on Computer Vision*, pages 707–723. Springer, 2022. 3
- [5] Dmitry Baranchuk, Andrey Voynov, Ivan Rubachev, Valentin Khruikov, and Artem Babenko. Label-efficient semantic segmentation with diffusion models. In *International Conference on Learning Representations*, 2022. 1
- [6] Tim Brooks, Aleksander Holynski, and Alexei A Efros. Instructpix2pix: Learning to follow image editing instructions. *arXiv preprint arXiv:2211.09800*, 2022. 3, 8
- [7] Shoufa Chen, Peize Sun, Yibing Song, and Ping Luo. Diffusiondet: Diffusion model for object detection. *arXiv preprint arXiv:2211.09788*, 2022. 1
- [8] Yunjey Choi, Youngjung Uh, Jaejun Yoo, and Jung-Woo Ha. Stargan v2: Diverse image synthesis for multiple domains. In *Proceedings of the IEEE Conference on Computer Vision and Pattern Recognition*, 2020. 7
- [9] Jia Deng, Wei Dong, Richard Socher, Li-Jia Li, Kai Li, and Li Fei-Fei. Imagenet: A large-scale hierarchical image database. In *Computer Vision and Pattern Recognition, 2009. CVPR 2009. IEEE Conference on*, pages 248–255. IEEE, 2009. 7
- [10] Tim Dockhorn, Arash Vahdat, and Karsten Kreis. GENIE: Higher-Order Denoising Diffusion Solvers. In *Advances in Neural Information Processing Systems*, 2022. 2
- [11] Rinon Gal, Yuval Alaluf, Yuval Atzmon, Or Patashnik, Amit H. Bermano, Gal Chechik, and Daniel Cohen-Or. An

- image is worth one word: Personalizing text-to-image generation using textual inversion, 2022. [3](#)
- [12] Rinon Gal, Or Patashnik, Haggai Maron, Gal Chechik, and Daniel Cohen-Or. Stylegan-nada: Clip-guided domain adaptation of image generators, 2021. [2](#), [3](#), [6](#), [12](#)
- [13] Ian Goodfellow, Jean Pouget-Abadie, Mehdi Mirza, Bing Xu, David Warde-Farley, Sherjil Ozair, Aaron Courville, and Yoshua Bengio. Generative adversarial nets. In Z. Ghahramani, M. Welling, C. Cortes, N. Lawrence, and K.Q. Weinberger, editors, *Advances in Neural Information Processing Systems*, volume 27. Curran Associates, Inc., 2014. [2](#)
- [14] Amir Hertz, Ron Mokady, Jay Tenenbaum, Kfir Aberman, Yael Pritch, and Daniel Cohen-Or. Prompt-to-prompt image editing with cross attention control. 2022. [3](#)
- [15] Jonathan Ho, Ajay Jain, and Pieter Abbeel. Denoising diffusion probabilistic models. In H. Larochelle, M. Ranzato, R. Hadsell, M.F. Balcan, and H. Lin, editors, *Advances in Neural Information Processing Systems*, volume 33, pages 6840–6851. Curran Associates, Inc., 2020. [1](#), [2](#), [12](#)
- [16] Tero Karras, Timo Aila, Samuli Laine, and Jaakko Lehtinen. Progressive growing of GANs for improved quality, stability, and variation. In *International Conference on Learning Representations*, 2018. [7](#)
- [17] Tero Karras, Miika Aittala, Timo Aila, and Samuli Laine. Elucidating the design space of diffusion-based generative models. In *Proc. NeurIPS*, 2022. [2](#)
- [18] Tero Karras, Miika Aittala, Samuli Laine, Erik Härkönen, Janne Hellsten, Jaakko Lehtinen, and Timo Aila. Alias-free generative adversarial networks. In *Proc. NeurIPS*, 2021. [2](#)
- [19] Tero Karras, Samuli Laine, Miika Aittala, Janne Hellsten, Jaakko Lehtinen, and Timo Aila. Analyzing and improving the image quality of StyleGAN. In *Proc. CVPR*, 2020. [2](#), [6](#)
- [20] Gwanghyun Kim, Taesung Kwon, and Jong Chul Ye. Diffusionclip: Text-guided diffusion models for robust image manipulation. In *Proceedings of the IEEE/CVF Conference on Computer Vision and Pattern Recognition*, pages 2426–2435, 2022. [2](#), [3](#), [12](#), [14](#)
- [21] Diederik P. Kingma and Max Welling. An introduction to variational autoencoders. *Foundations and Trends® in Machine Learning*, 12(4):307–392, 2019. [2](#)
- [22] Vladimir Kulikov, Shahar Yadin, Matan Kleiner, and Tomer Michaeli. Sinddm: A single image denoising diffusion model. *arXiv preprint arXiv:2211.16582*, 2022. [3](#)
- [23] Mingi Kwon, Jaeseok Jeong, and Youngjung Uh. Diffusion models already have a semantic latent space. In *The Eleventh International Conference on Learning Representations*, 2023. [2](#), [3](#), [7](#)
- [24] Tsung-Yi Lin, Michael Maire, Serge J. Belongie, Lubomir D. Bourdev, Ross B. Girshick, James Hays, Pietro Perona, Deva Ramanan, Piotr Dollár, and C. Lawrence Zitnick. Microsoft COCO: common objects in context. *CoRR*, abs/1405.0312, 2014. [1](#)
- [25] Cheng Lu, Yuhao Zhou, Fan Bao, Jianfei Chen, Chongxuan Li, and Jun Zhu. DPM-solver: A fast ODE solver for diffusion probabilistic model sampling in around 10 steps. In Alice H. Oh, Alekh Agarwal, Danielle Belgrave, and Kyunghyun Cho, editors, *Advances in Neural Information Processing Systems*, 2022. [2](#)
- [26] Andreas Lugmayr, Martin Danelljan, Andrés Romero, Fisher Yu, Radu Timofte, and Luc Van Gool. Repaint: Inpainting using denoising diffusion probabilistic models. In *CVPR*, pages 11451–11461. IEEE, 2022. [1](#)
- [27] Anish Mittal, Rajiv Soundararajan, and Alan C. Bovik. Making a “completely blind” image quality analyzer. *IEEE Signal Processing Letters*, 20(3):209–212, 2013. [5](#)
- [28] Ron Mokady, Amir Hertz, Kfir Aberman, Yael Pritch, and Daniel Cohen-Or. Null-text inversion for editing real images using guided diffusion models, 2022. [3](#), [8](#)
- [29] Alexander Quinn Nichol and Prafulla Dhariwal. Improved denoising diffusion probabilistic models. In Marina Meila and Tong Zhang, editors, *Proceedings of the 38th International Conference on Machine Learning*, volume 139 of *Proceedings of Machine Learning Research*, pages 8162–8171. PMLR, 18–24 Jul 2021. [12](#)
- [30] Alexander Quinn Nichol, Prafulla Dhariwal, Aditya Ramesh, Pranav Shyam, Pamela Mishkin, Bob McGrew, Ilya Sutskever, and Mark Chen. GLIDE: Towards photorealistic image generation and editing with text-guided diffusion models. In Kamalika Chaudhuri, Stefanie Jegelka, Le Song, Csaba Szepesvari, Gang Niu, and Sivan Sabato, editors, *Proceedings of the 39th International Conference on Machine Learning*, volume 162 of *Proceedings of Machine Learning Research*, pages 16784–16804. PMLR, 17–23 Jul 2022. [3](#)
- [31] Or Patashnik, Zongze Wu, Eli Shechtman, Daniel Cohen-Or, and Dani Lischinski. Styleclip: Text-driven manipulation of stylegan imagery. In *Proceedings of the IEEE/CVF International Conference on Computer Vision (ICCV)*, pages 2085–2094, October 2021. [2](#), [3](#), [7](#)
- [32] Alec Radford, Jong Wook Kim, Chris Hallacy, Aditya Ramesh, Gabriel Goh, Sandhini Agarwal, Girish Sastry, Amanda Askell, Pamela Mishkin, Jack Clark, Gretchen Krueger, and Ilya Sutskever. Learning transferable visual models from natural language supervision. In Marina Meila and Tong Zhang, editors, *Proceedings of the 38th International Conference on Machine Learning*, volume 139 of *Proceedings of Machine Learning Research*. PMLR, 18–24 Jul 2021. [3](#)
- [33] Aditya Ramesh, Prafulla Dhariwal, Alex Nichol, Casey Chu, and Mark Chen. Hierarchical text-conditional image generation with CLIP latents. *CoRR*, abs/2204.06125, 2022. [1](#), [3](#)
- [34] Robin Rombach, Andreas Blattmann, Dominik Lorenz, Patrick Esser, and Björn Ommer. High-resolution image synthesis with latent diffusion models. In *Proceedings of the IEEE/CVF Conference on Computer Vision and Pattern Recognition*, pages 10684–10695, 2022. [1](#), [3](#), [8](#)
- [35] Nataniel Ruiz, Yuanzhen Li, Varun Jampani, Yael Pritch, Michael Rubinstein, and Kfir Aberman. Dreambooth: Fine tuning text-to-image diffusion models for subject-driven generation. 2022. [3](#)
- [36] Chitwan Saharia, William Chan, Saurabh Saxena, Lala Li, Jay Whang, Emily Denton, Seyed Kamyar Seyed Ghasemipour, Raphael Gontijo-Lopes, Burcu Karagol Ayan, Tim Salimans, Jonathan Ho, David J. Fleet, and Mohammad Norouzi. Photorealistic text-to-image diffusion models with deep language

- understanding. In Alice H. Oh, Alekh Agarwal, Danielle Belgrave, and Kyunghyun Cho, editors, *Advances in Neural Information Processing Systems*, 2022. 1, 3
- [37] Chitwan Saharia, Jonathan Ho, William Chan, Tim Salimans, David J Fleet, and Mohammad Norouzi. Image super-resolution via iterative refinement. *arXiv:2104.07636*, 2021. 1
- [38] Christoph Schuhmann, Romain Beaumont, Richard Vencu, Cade W Gordon, Ross Wightman, Mehdi Cherti, Theo Coombes, Aarush Katta, Clayton Mullis, Mitchell Wortsman, Patrick Schramowski, Srivatsa R Kundurthy, Katherine Crowson, Ludwig Schmidt, Robert Kaczmarczyk, and Jenia Jitsev. LAION-5b: An open large-scale dataset for training next generation image-text models. In *Thirty-sixth Conference on Neural Information Processing Systems Datasets and Benchmarks Track*, 2022. 1
- [39] Jiaming Song, Chenlin Meng, and Stefano Ermon. Denoising diffusion implicit models. In *International Conference on Learning Representations*, 2021. 1, 2
- [40] Yang Song, Jascha Sohl-Dickstein, Diederik P Kingma, Abhishek Kumar, Stefano Ermon, and Ben Poole. Score-based generative modeling through stochastic differential equations. In *International Conference on Learning Representations*, 2021. 2
- [41] Omer Tov, Yuval Alaluf, Yotam Nitzan, Or Patashnik, and Daniel Cohen-Or. Designing an encoder for stylegan image manipulation. *ACM Transactions on Graphics (TOG)*, 40(4):1–14, 2021. 2, 7
- [42] Dani Valevski, Matan Kalman, Y. Matias, and Yaniv Leviathan. Unitune: Text-driven image editing by fine tuning an image generation model on a single image. *ArXiv*, abs/2210.09477, 2022. 3
- [43] Weilun Wang, Jianmin Bao, Wengang Zhou, Dongdong Chen, Dong Chen, Lu Yuan, and Houqiang Li. Sindiffusion: Learning a diffusion model from a single natural image. *arXiv preprint arXiv:2211.12445*, 2022. 3
- [44] Daniel Watson, Jonathan Ho, Mohammad Norouzi, and William Chan. Learning to efficiently sample from diffusion probabilistic models, 2022. 2
- [45] Fisher Yu, Yinda Zhang, Shuran Song, Ari Seff, and Jianxiong Xiao. Lsun: Construction of a large-scale image dataset using deep learning with humans in the loop. *arXiv preprint arXiv:1506.03365*, 2015. 7
- [46] Zhixing Zhang, Ligong Han, Arnab Ghosh, Dimitris Metaxas, and Jian Ren. Sine: Single image editing with text-to-image diffusion models. *arXiv preprint arXiv:2212.04489*, 2022. 3

Appendix

A. Training algorithm

(Red) represents the snippets of the DiffusionCLIP procedure that are replaced with the proposed modifications in Section 3.1 and Section 3.2 (Green).

Algorithm 1: Training procedure. **DiffusionCLIP** vs **Ours**.

```

Input :  $\epsilon_\theta, n_{iter}, x_0, y_{ref}, y_{tar}, \tau_{enc}, \tau_{dec}$ 
Output :  $\epsilon_{\hat{\theta}}$ 
/* Encoding process */
for  $\tau = 0, \dots, \tau_{enc}$  do
     $x_0(\tau; \theta) = x_\tau - \sqrt{1 - \alpha_\tau} \cdot \epsilon_\theta(x_\tau) / \sqrt{\alpha_\tau}$ 
     $x_{\tau+1}(\theta) = \sqrt{\alpha_{\tau+1}} \cdot x_0^\tau(\theta) + \sqrt{1 - \alpha_{\tau+1}} \epsilon_{\hat{\theta}}(x_\tau)$ 
end
 $x_{t_0} = \sqrt{\alpha_{t_0}} x_0 + \sqrt{1 - \alpha_{t_0}} I$ 
 $\hat{\theta} = \theta$ 
for  $i = 1, \dots, n_{iter}$  do
    /* Decoding process and model update */
    for  $\tau = \tau_{dec}, \dots, 1$  do
         $x_0(\tau; \hat{\theta}) = x_\tau - \sqrt{1 - \alpha_\tau} \cdot \epsilon_{\hat{\theta}}(x_\tau) / \sqrt{\alpha_\tau}$ 
         $x_{\tau-1}(\hat{\theta}) = \sqrt{\alpha_{\tau-1}} \cdot x_0^\tau(\hat{\theta}) + \sqrt{1 - \alpha_{\tau-1}} \epsilon_{\hat{\theta}}(x_\tau)$ 
    end
     $\hat{\theta} = \hat{\theta} + \nabla_{\hat{\theta}} \mathcal{L}(x_0(\hat{\theta}), y_{tar}, x_0, y_{ref})$ 
     $x_0(t_0; \hat{\theta}) = (x_{t_0} - \sqrt{1 - \alpha_{t_0}} \epsilon_\theta(x_{t_0}, t_0)) / \sqrt{\alpha_{t_0}}$ 
     $\hat{\theta} = \hat{\theta} + \nabla_{\hat{\theta}} \mathcal{L}(x_0(t_0; \hat{\theta}), y_{tar}, x_0, y_{ref})$ 
end
return  $\epsilon_{\hat{\theta}}$ 

```

B. Technical setup

All experiments are performed on a single Tesla A100 GPU. 64 CPU cores are used. PyTorch version is 1.10.1.

We use the following architectures of the diffusion models: [15] for Celeba-HQ-256, [29] for LSUN-church-256, AFHQ-dog-256 and ImageNet-512.

C. Evaluation of stochastic encoding

In this section, we compare stochastic (DDPM) and deterministic (DDIM) encoding methods using the mean opinion score. We ask assessors to estimate how the reconstructed image is similar to the reference one according to the criteria in Table 4 (Bottom).

According to the human opinion in Table 4 (Top), for $t_0 = 300$, DDPM encoding does not affect semantic attributes noticeably. Thus, our method considers lower $t_0 \leq 300$ for shallow image manipulations, e.g., “Makeup face”, where preserving most details of the original image is important. On the other hand, $t_0 = 500$ slightly alters the face attributes. Therefore, we use $t_0=350-500$ for severe transforms, e.g., “Zombie”, that significantly affect the semantic attributes.

t_0	100	300	500
DDPM	4.58	4.08	3.40
DDIM	4.75	4.46	4.40

Criterion
5: Looks identical. No visible changes or artifacts.
4: Minor visible changes. All face attributes are fully preserved.
3: Minor changes of the face attributes. The person is the same.
2: Significant changes of the face attributes.
1: Completely different person.

Table 4: (Top) Comparison of stochastic (DDPM) and deterministic (DDIM) encoding methods for different steps t_0 in terms of mean opinion score that measures similarity between reconstructed and original images. (Bottom) The criteria which were shown to assessors for estimation.

D. List of textual transforms

D.1. Prelearned image manipulations

For the human evaluation, we use the following established transformations [20, 12]:

- **Celeba-HQ-256** — “Face” → “Angry face”, “Face” → “Pale face”, “Face” → “Smiling Face”, “Photo” → “Painting in Fernando Botero style”, “Person” → “Nicolas Cage”, “Photo” → “Painting in Cubism style”, “Face” → “Makeup face”, “Photo” → “Painting in Modigliani style”, “Human” → “Neanderthal”, “Person” → “Old person”, “Human” → “3D rendering in style of Pixar”, “Person” → “Surprised”, “Face” → “Tanned face”, “Photo” → “Watercolor art”, “Human” → “Zombie”, “Person” → “Mark Zuckerberg”.
- **LSUN-church-256** — “Church” → “Golden church, Church” → “Colorful church”, “Church” → “Gothic church, “Church” → “Modern architecture”, “Church” → “Snow covered church”, “Church” → “Ancient temple”.
- **AFHQ-dog-256** — “Dog” → “Angry dog”, “Dog” → “Anime dog”, “Dog” → “Bear”, “Dog” → “Fox”, “Dog” → “Smiling dog”, “Dog to Zombie dog”.
- **ImageNet-512** — “Photo” → “Painting in cubism style”, “Photo” → “Painting in cubism style”, “Photo” → “Painting in Van Gogh style”, “Photo” → “Painting in pointilism style”, “Photo” → “Sketch”, “Photo” → “Watercolor art”.

D.2. Single image editing

- **In-domain** transforms — “Face” → “Angry face”, “Person” → “Nicolas Cage”, “Face” → “Makeup face”, “Person” → “Old person”, “Person” → “Surprised”, “Man” → “Woman” (or vice versa), “Face” → “Smiling face”, “Person” → “Mark Zuckerberg”.

- **Out-of-domain** transforms — “Human” → “3D rendering in style of Pixar”, “Human” → “Neanderthal”, “Photo” → “Painting in Fernando Botero style”, “Photo” → “Painting in Modigliani style”, “Photo” → “Self portrait by Frida Kahlo”, “Photo” → “Sketch”, “Human” → “Jocker”, “Human” → “Zombie”.

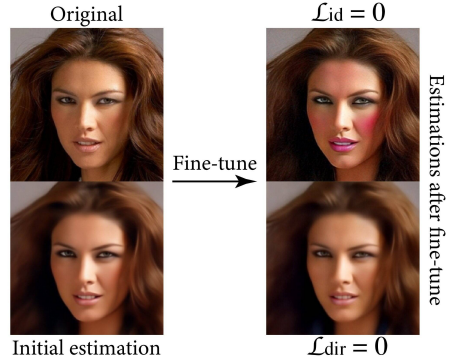


Figure 11: The x_0 estimates before and after finetuning using \mathcal{L}_{dir} and \mathcal{L}_{id} losses, independently. Opposed to \mathcal{L}_{dir} , \mathcal{L}_{id} does not improve the perceptual quality of the estimates.

Text description	lr	λ	t_0
CelebA-HQ-256			
Angry face	$3e-6$	0.6	300
Pale face	$3e-6$	0.6	300
Smiling face	$3e-6$	0.6	300
Painting in Fernando Botero style	$8e-6$	0.3	450
Nicolas Cage	$7e-6$	0.1	450
Painting in Cubism style	$7e-6$	0.1	450
Makeup face	$1e-6$	0.9	300
Painting in Modigliani style	$5e-6$	0.4	450
Neanderthal	$6e-6$	0.3	450
Old person	$5e-6$	0.2	380
3D rendering in style of Pixar	$3e-6$	0.1	450
Surprised	$4e-6$	0.8	450
Tanned face	$4e-6$	0.8	450
Watercolor art	$6e-6$	0.5	450
Zombie	$2e-5$	0.1	430
Mark Zuckerberg	$2e-6$	0.3	400
LSUN-Church-256			
Golden church	$3e-6$	0.1	380
Colorful church	$3e-6$	0.0	400
Gothic church	$3e-6$	0.1	380
Modern architecture	$2e-6$	0.2	400
Snow covered church	$3e-6$	0.6	400
Ancient temple	$4e-6$	0.8	400
AFHQ-Dog-256			
Angry dog	$6e-6$	0.8	380
Anime dog	$8e-6$	0.2	450
Bear	$8e-6$	0.7	450
Fox	$8e-6$	0.6	450
Smiling dog	$6e-6$	0.3	400
Zombie dog	$6e-6$	0.2	450
ImageNet-512			
Painting in cubism style	$8e-6$	0.1	450
Painting in cubism style	$8e-6$	0.1	450
Painting in Van Gogh style	$8e-6$	0.1	450
Painting in pointilism style	$8e-6$	0.2	450
Sketch	$8e-6$	0.1	450
Watercolor art	$6e-6$	0.1	450

Table 5: Hyperparameter values used to learn text-driven image manipulations. λ represents the coefficient in front of the \mathcal{L}_{id} term.

E. Quality improvement effect

The paper demonstrates that our adaptation procedure improves the perceptual quality of the approximate x_0 estimates at a time step t_0 .

In this experiment, we ensure that \mathcal{L}_{dir} (6) is indeed responsible for these changes but not \mathcal{L}_{id} (5). Figure 11 provides the visual examples of the x_0 estimates after the model finetuning independently using one of these losses. We observe that \mathcal{L}_{id} does not lead to perceptual quality improvements.



Figure 12: The effect of different hyperparameter values for a few transforms. $\lambda_{\mathcal{L}_{id}}$ corresponds to the coefficient in front of the regularization term.

F. Hyperparameters

The proposed approach is sensitive to hyperparameter values. In Table 5, we provide the full list of hyperparameter values used for different datasets and transforms. Figure 12



Figure 13: Visual examples of the failed image manipulations produced with our approach.

presents a few examples of image manipulations with different hyperparameter values. Below, we give a few recommendations to make the tuning of our method more approachable for users.

- Consider using higher values of the regularization coefficient λ (e.g., 5–10) for the shallow transforms like “Red hair”.
- Higher values of the t_0 allow us to make stronger transforms but can bring more irrelevant changes. Thus, we recommend to use smaller t_0 values ($t_0 = 200–350$) for the shallow transforms, e.g., “Makeup face”, “Surprised face”, and higher t_0 values ($t_0 = 350–500$) for the strong manipulations, e.g., “Zombie”, “Sketch”.
- We also find that a higher learning rate, e.g., $2e-5$, allows obtaining better results for the strong transforms, while for the shallow ones, smaller values are preferable, e.g., $5e-6$.

G. Failure cases

The proposed approach is limited by the capabilities of the CLIP and pretrained diffusion models. Sometimes, the former cannot provide the desired signal to adapt the diffusion model properly. In Figure 13, we provide a few visual examples of such text descriptions.

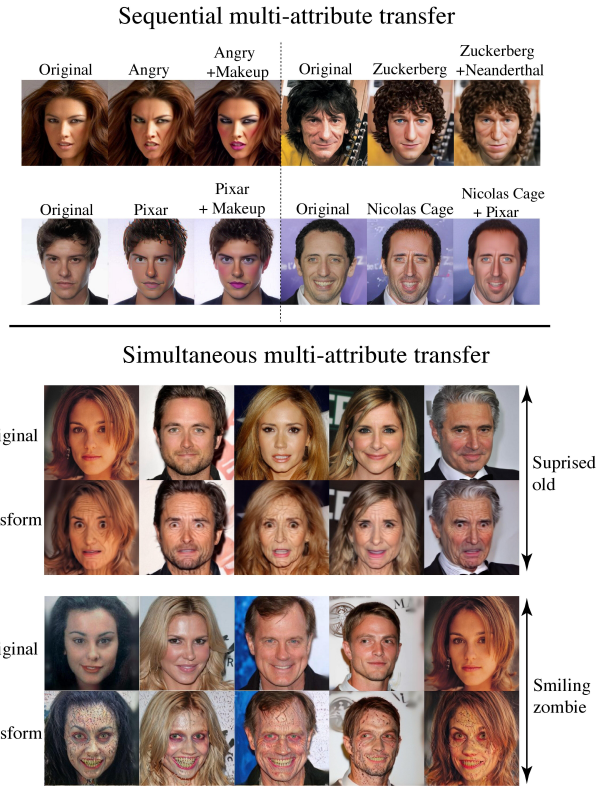


Figure 14: Visual examples of the multi-attribute transfer. **Sequential** setting adapts the model to two different text descriptions one by one. **Simultaneous** means that we form a single text description that combines two different attributes.

H. Multi-attribute transfer

Following [20], we also demonstrate that our approach is able to produce multi-attribute transfers in both sequential and simultaneous regimes. The visual examples of the learned image manipulations are presented in Figure 14.



Figure 15: Voting results for prelearned image manipulations (Top) and single-image editing (Bottom).

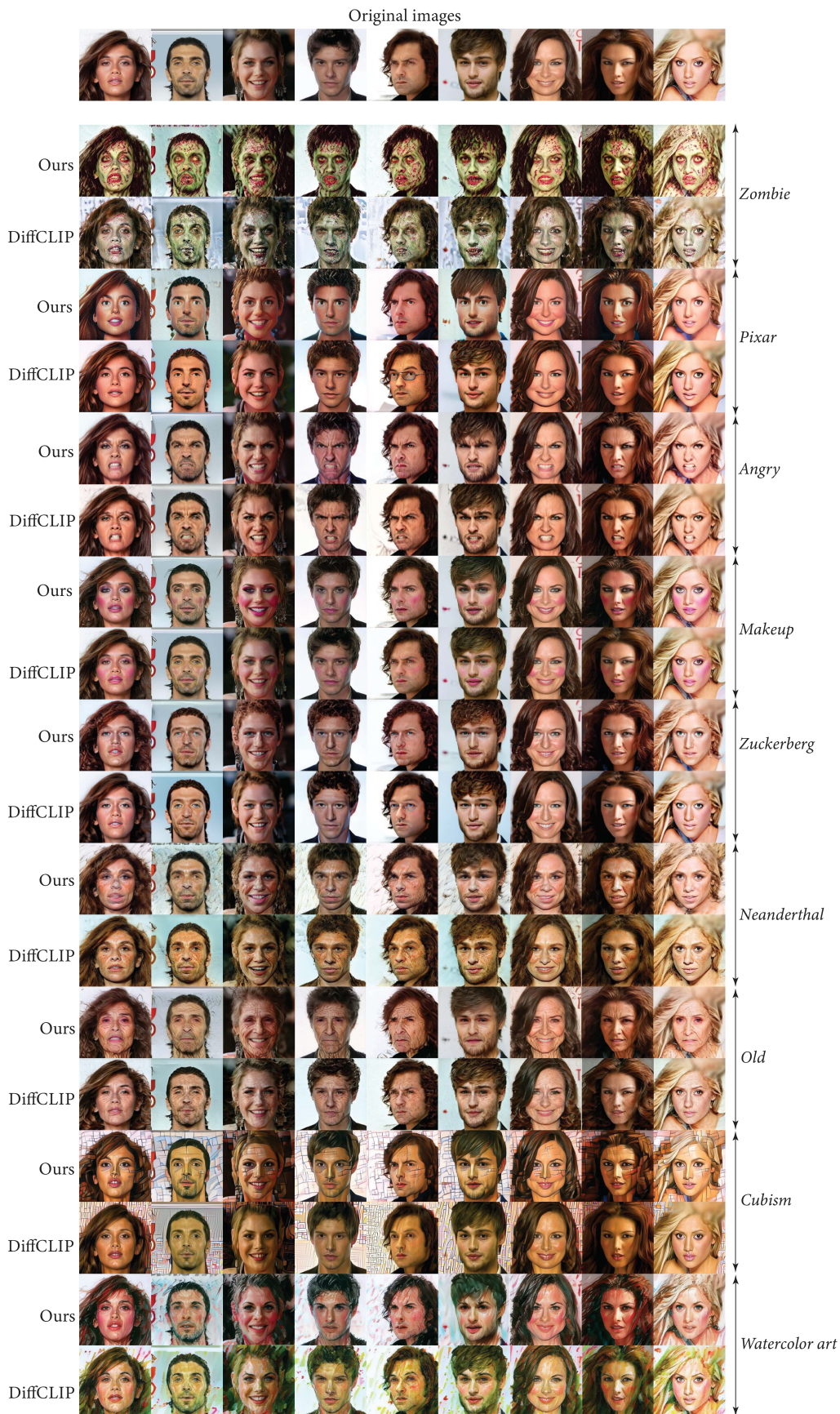


Figure 16: More visual examples of the prelearned image manipulations on CelebA-HQ-256 (Ours and DiffusionCLIP).

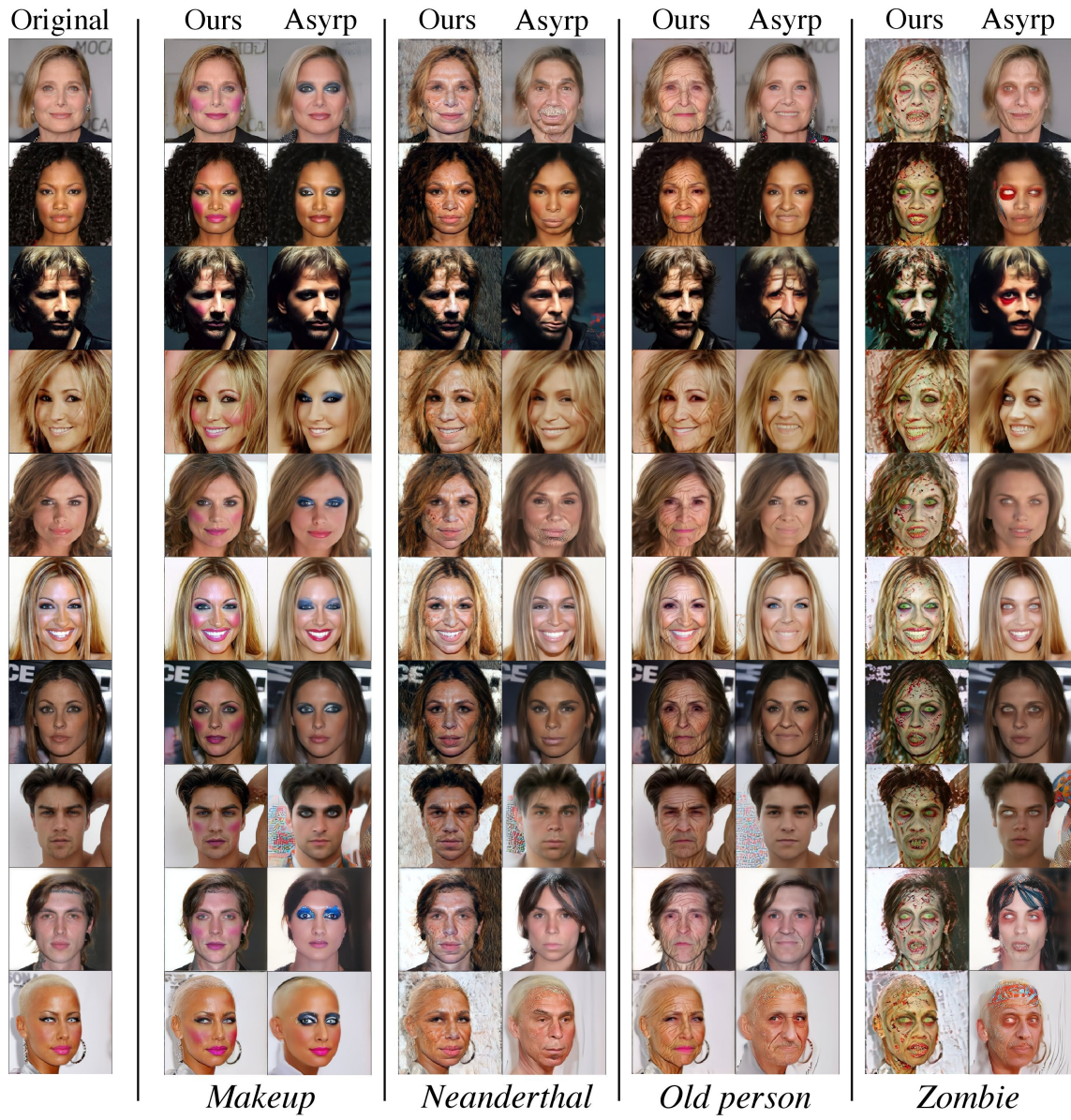


Figure 17: More visual examples of the prelearned image manipulations on CelebA-HQ-256 (Ours and Asyrp).

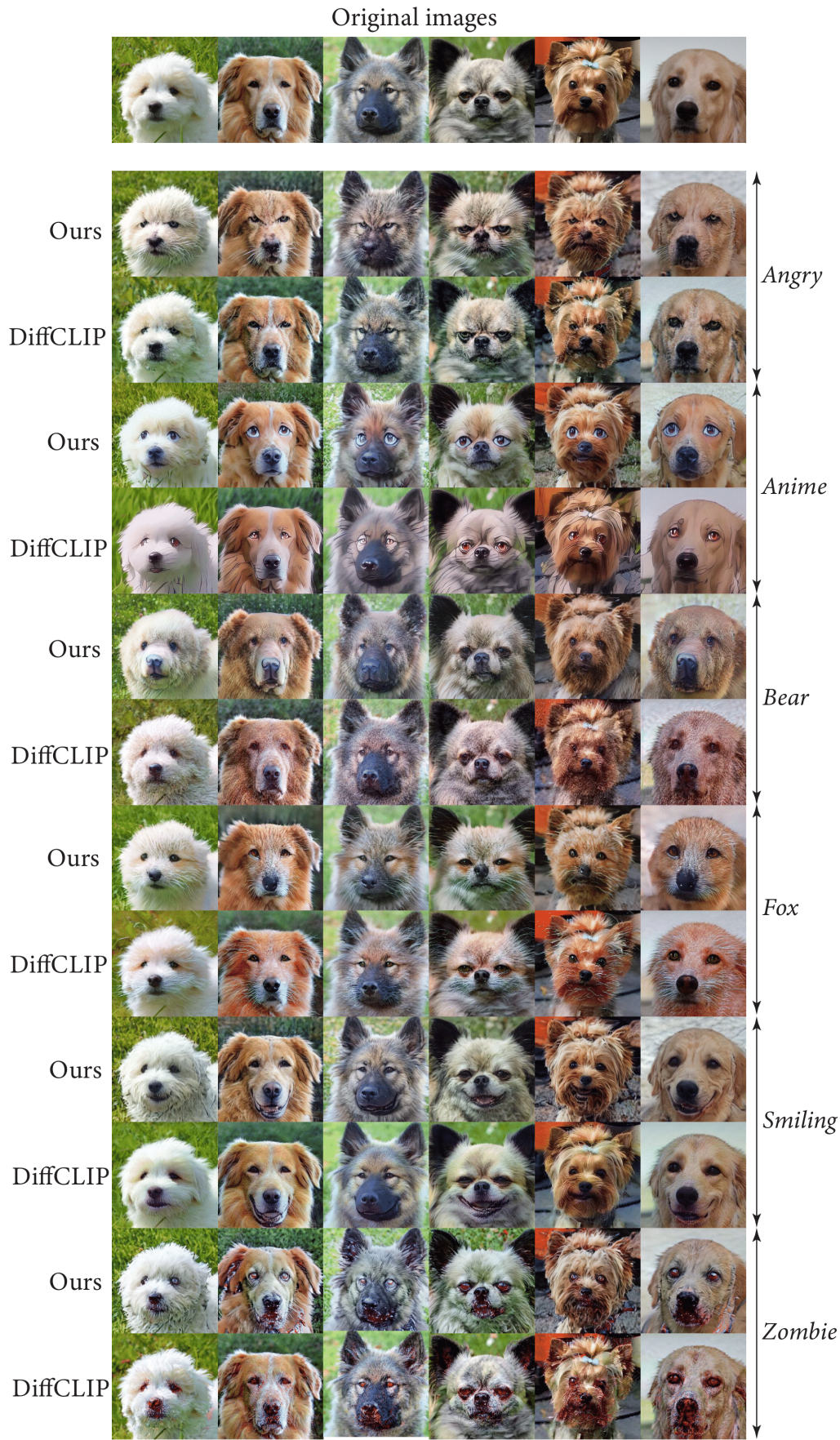


Figure 18: More visual examples of the prelearned image manipulations on AFHQ-Dogs-256 (Ours and DiffusionCLIP).

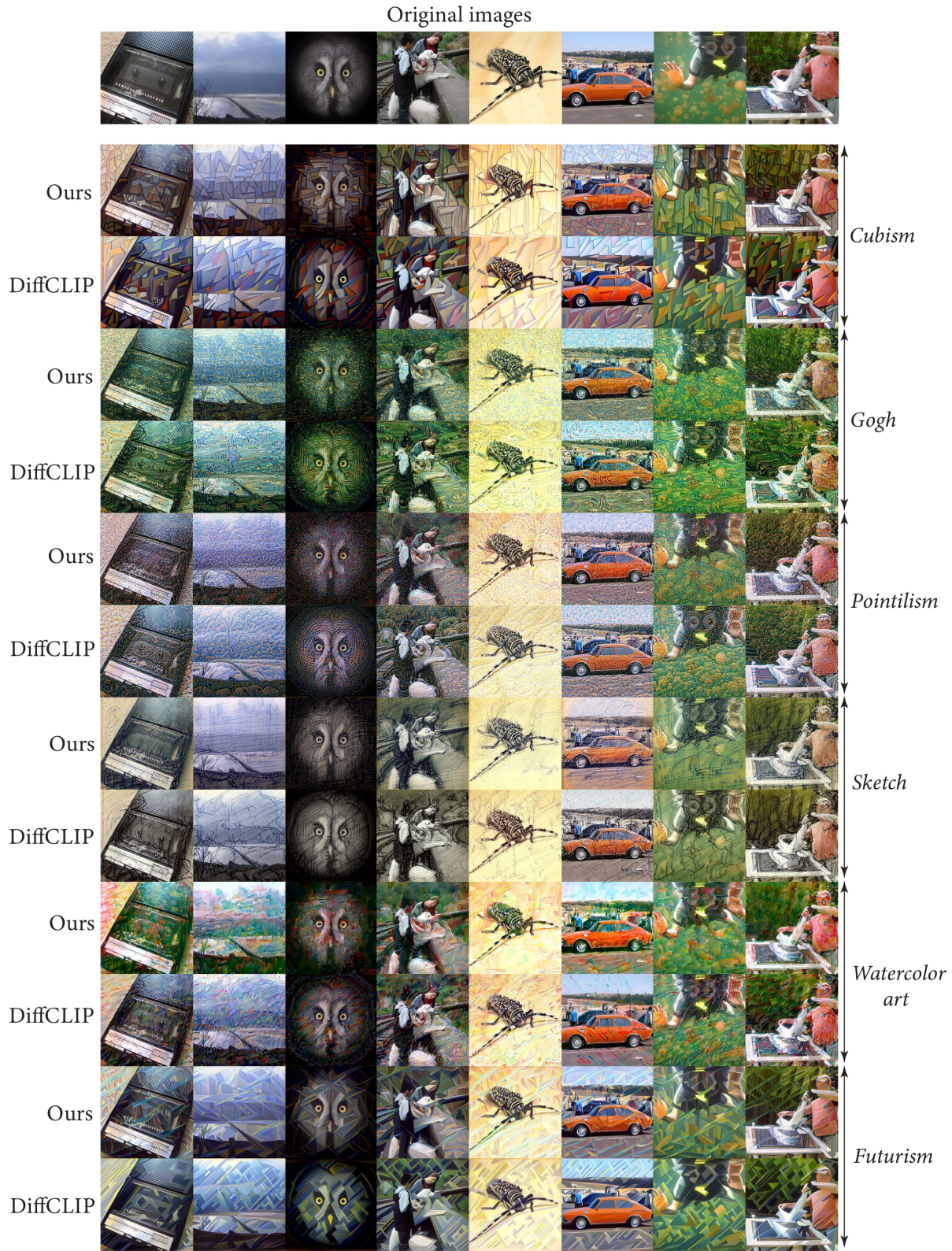


Figure 19: More visual examples of the prelearned image manipulations on ImageNet-512 (Ours and DiffusionCLIP).

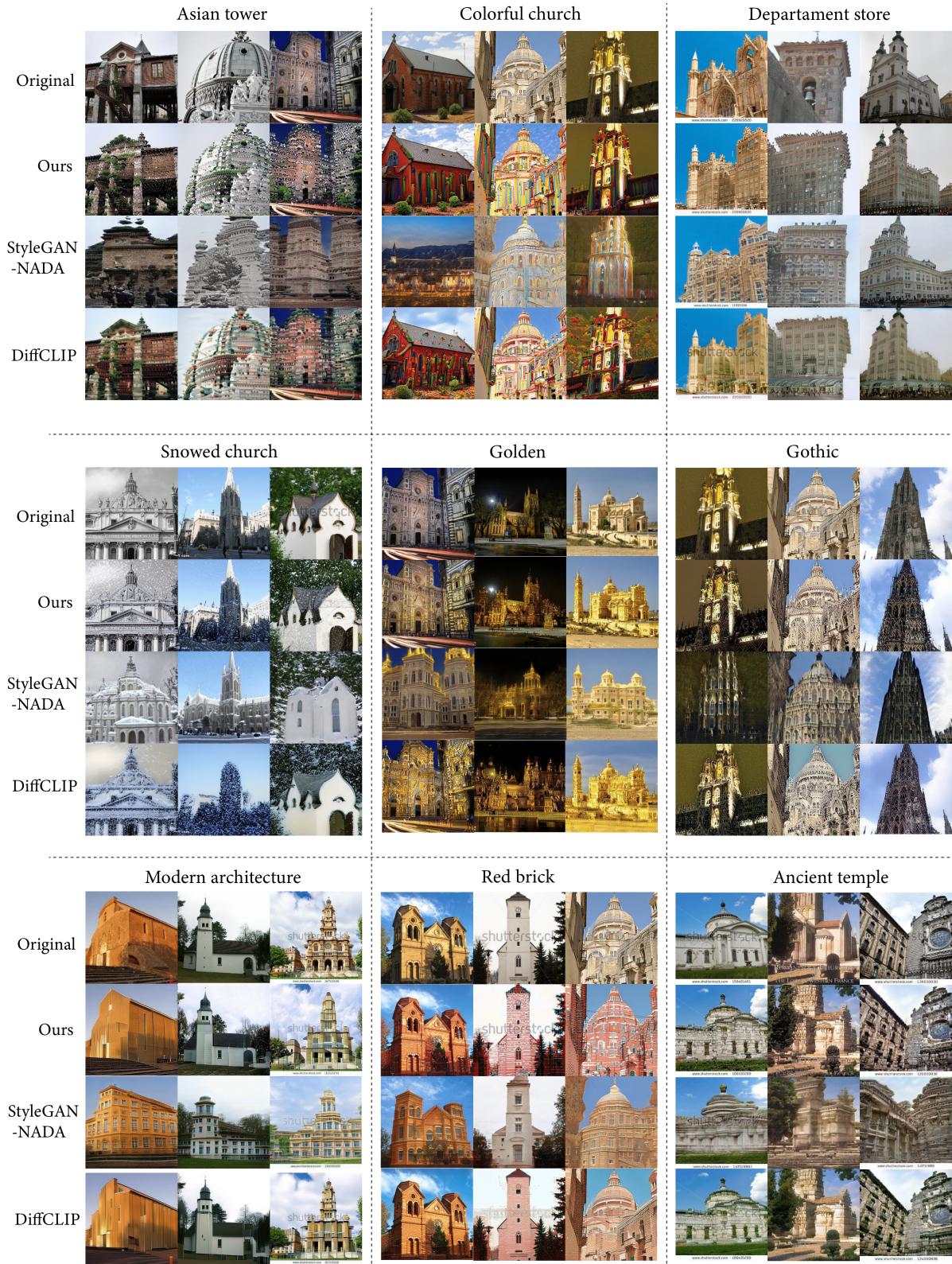


Figure 20: More visual examples of the prelearned image manipulations on LSUN-Church-256 (Ours, DiffusionCLIP and StyleGAN-NADA).

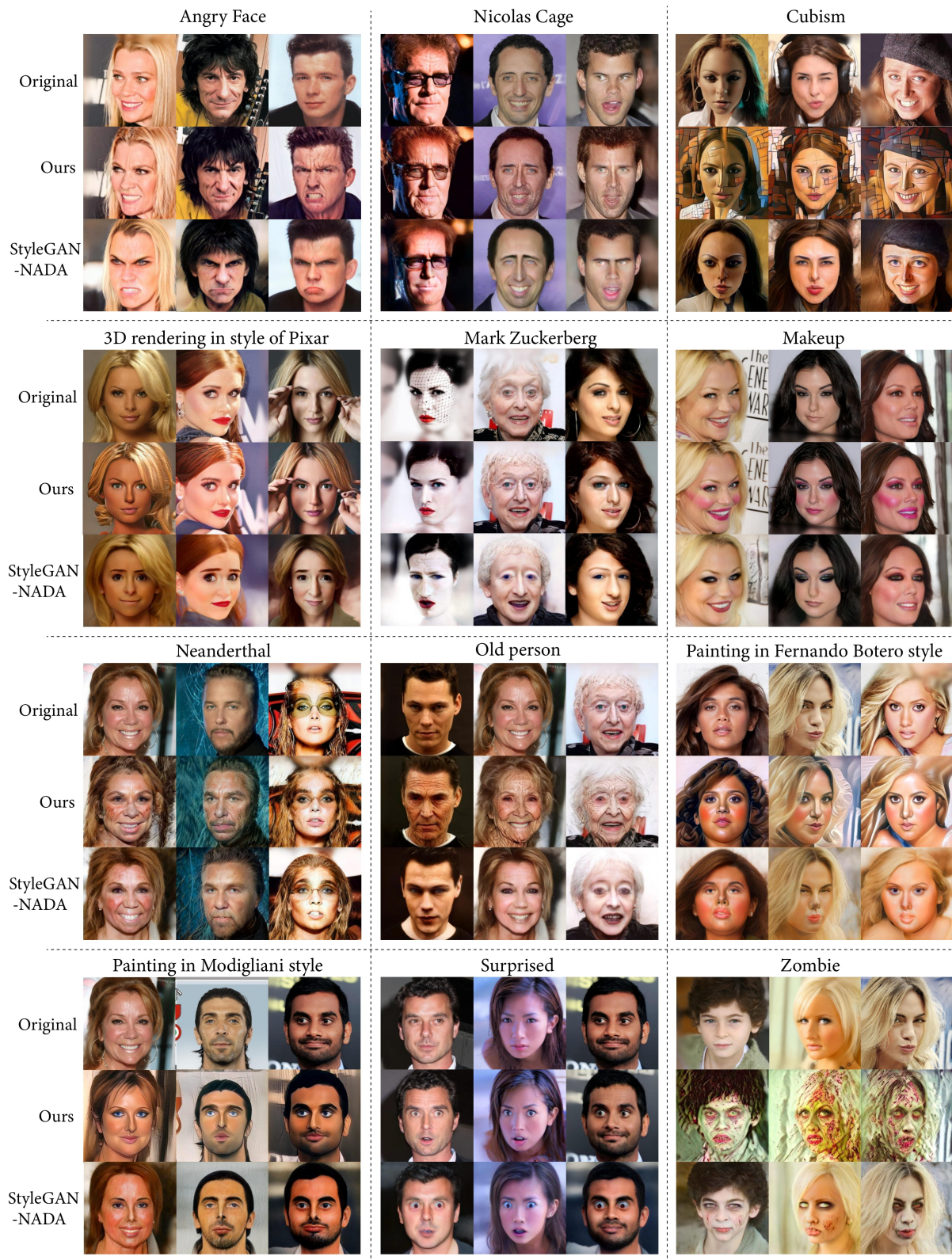


Figure 21: More visual examples of the prelearned image manipulations on CelebA-HQ-256 (Ours and StyleGAN-NADA).

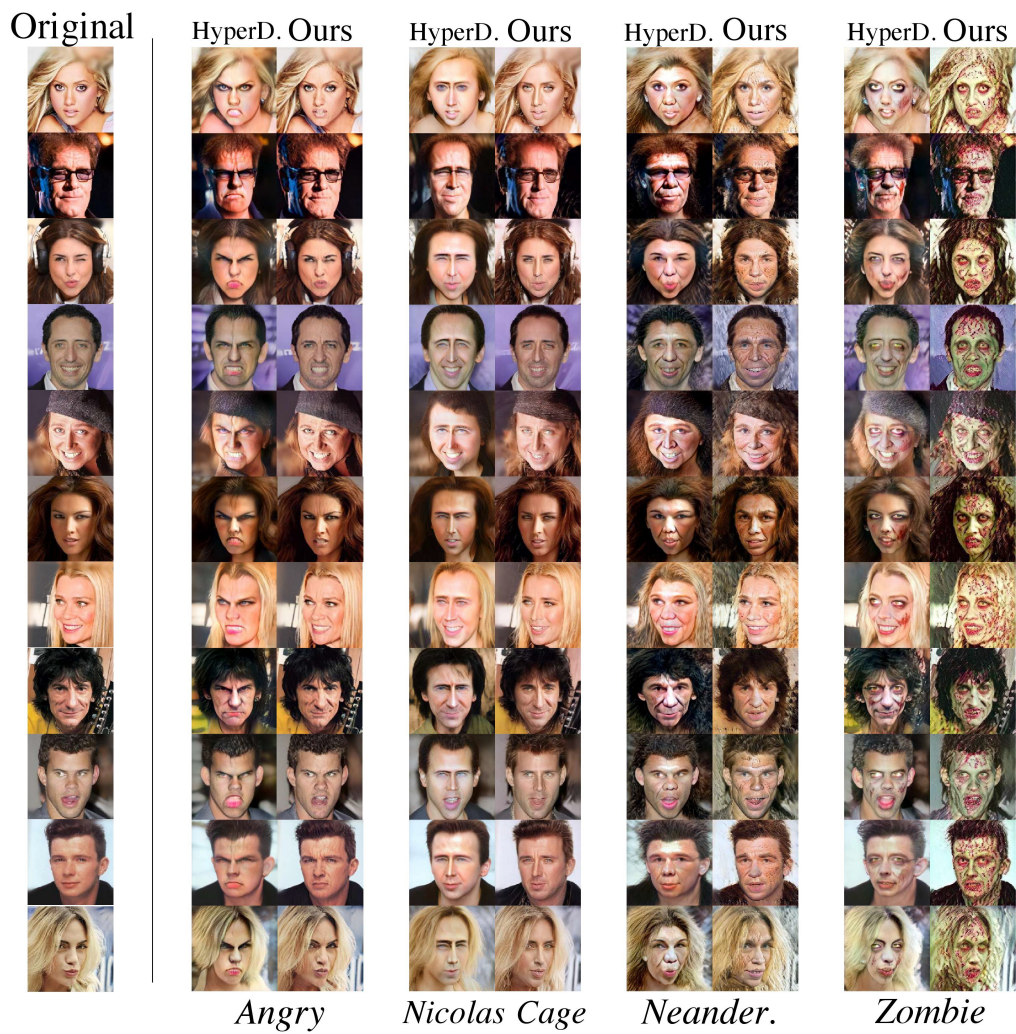


Figure 22: More visual examples of the prelearned image manipulations on CelebA-HQ-256 (Ours and HyperDomainNet).

Original images



Transformed images

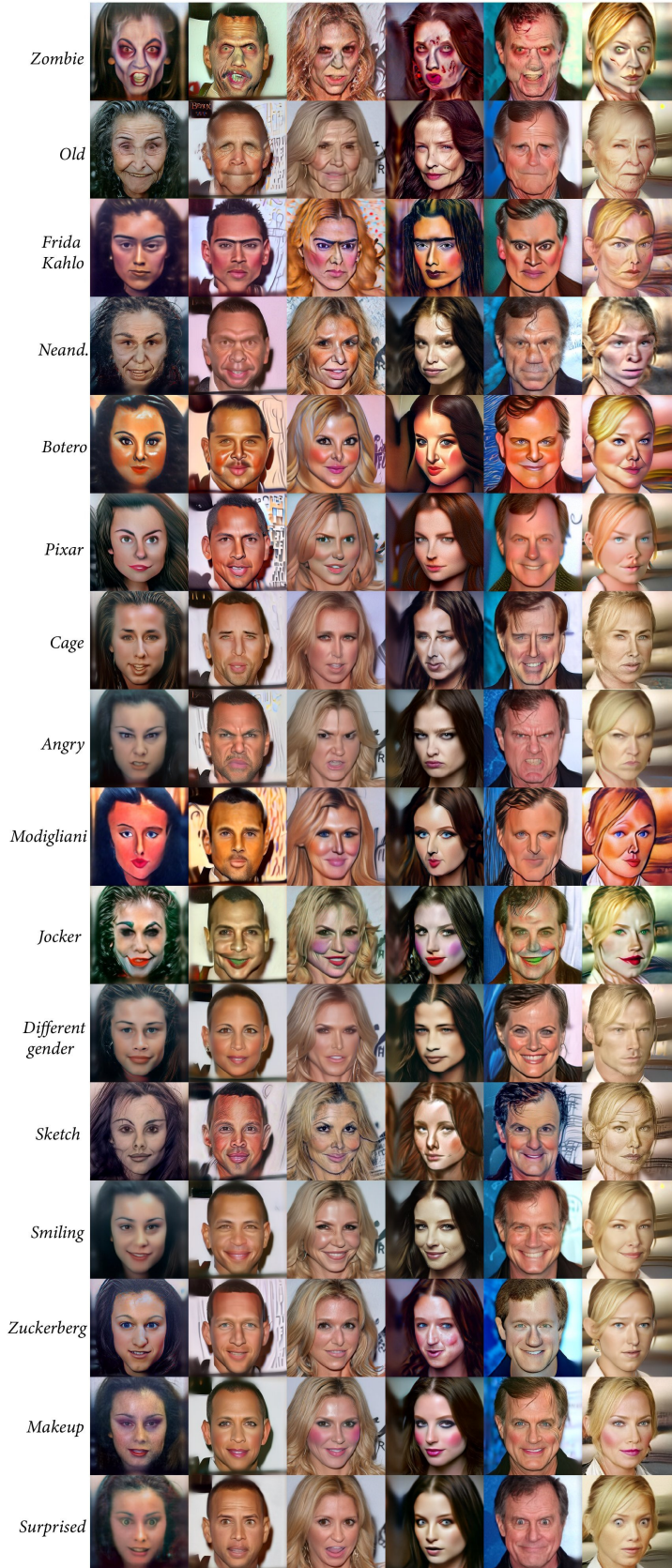


Figure 23: More visual examples of the text-guided single-image editing produced with our method.

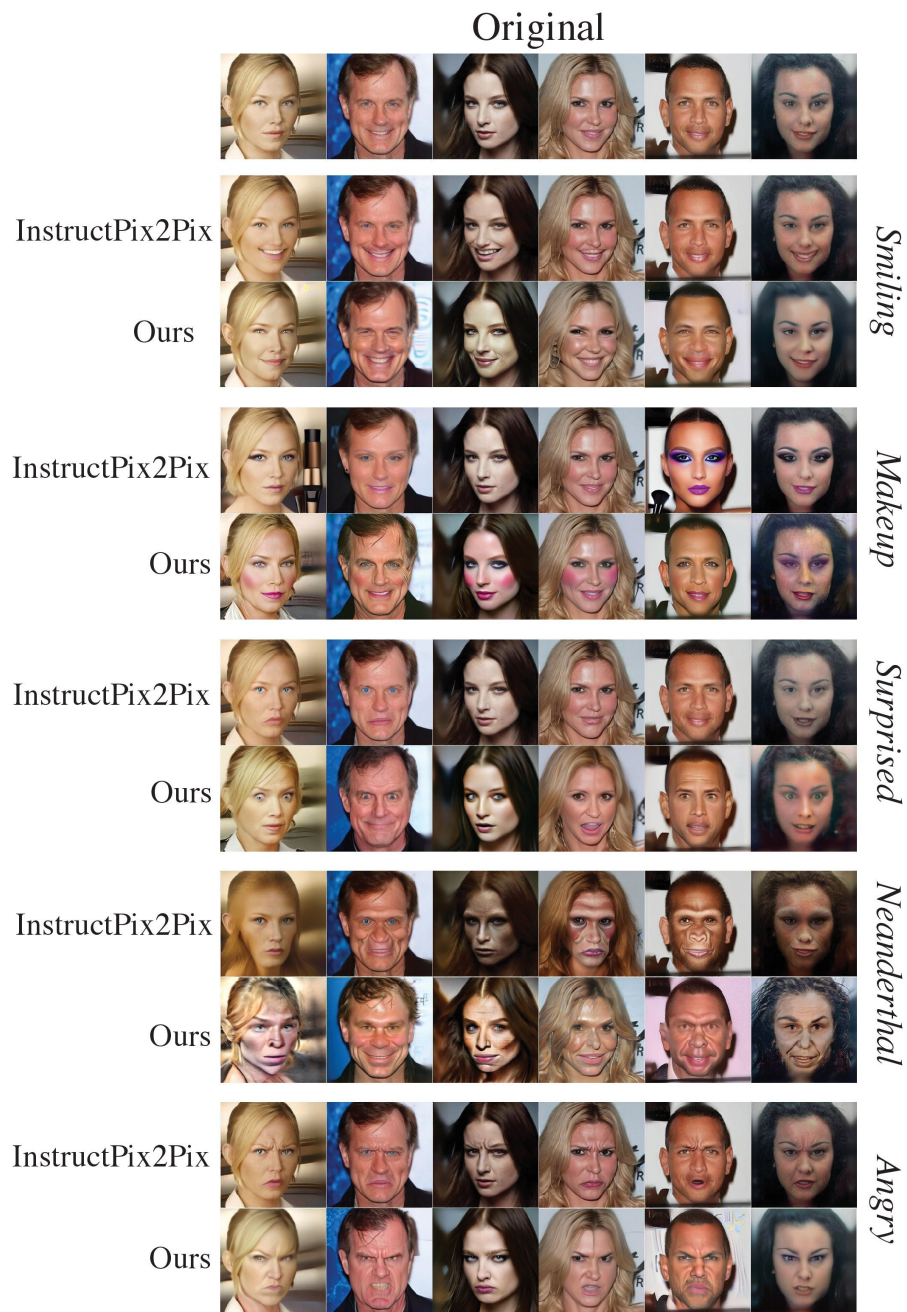


Figure 24: More visual examples of the text-guided single-image editing (Ours and InstructPix2Pix).